

Safe Navigation of Bipedal Robots via Koopman Operator-Based Model Predictive Control

Jeonghwan Kim, Yunhai Han, Harish Ravichandar, Sehoon Ha

Abstract—Nonlinearity in dynamics has long been a major challenge in robotics, often causing significant performance degradation in existing control algorithms. For example, the navigation of bipedal robots can exhibit nonlinear behaviors even under simple velocity commands, as their actual dynamics are governed by complex whole-body movements and discrete contacts. In this work, we propose a novel safe navigation framework inspired by Koopman operator theory. We first train a low-level locomotion policy using deep reinforcement learning, and then capture its low-frequency, base-level dynamics by learning linearized dynamics in a high-dimensional lifted space using Dynamic Mode Decomposition. Then, our model-predictive controller (MPC) efficiently optimizes control signals via standard quadratic objective and the linear dynamics constraint in the lifted space. We demonstrate that the Koopman-based model more accurately predicts bipedal robot trajectories than baseline approaches. Furthermore, we show that the proposed navigation framework achieves improved safety with better success rates in dense environments with narrow passages.

I. INTRODUCTION

Nonlinear dynamics have long been a fundamental challenge in robotics, which often leads to significant difficulties in modeling, prediction, and control. Legged robot navigation is one of the examples because even simple velocity commands can induce highly nonlinear behaviors due to its complex hybrid dynamics. Researchers have explored both model-based and learning-based approaches. Model-based methods often integrate obstacle avoidance constraints with model predictive control (MPC), leveraging explicit dynamic models for safe navigation [1]–[4]. On the other hand, learning-based frameworks have achieved impressive results in quadrupedal locomotion and navigation, either by training high-level policies [5]–[7] or developing end-to-end policies [8]–[10]. While both lines of research have been successful, model-based approaches are constrained by the complexity of accurate dynamics modeling and the increased computation cost, whereas learning-based methods demand extensive training data and tend to show degraded performance in unseen environments.

Researchers have explored various algorithms that combine the strengths of both model-based and learning-based approaches [11], [12]. A notable example is the work of Li et al. [13], which identifies low-dimensional linear models of RL-based closed-loop dynamics in legged robots via system identification. Their results demonstrate that the learned models can successfully enable safety-critical optimal control, such as MPC with control barrier functions, on physical systems. However, this method learns

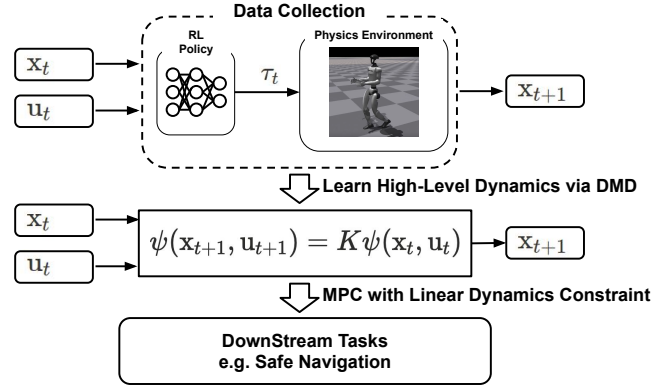


Fig. 1: Our approach first trains a locomotion controller on a bipedal robot and then learns the linearized high-level dynamics using Koopman operator theory. Once the dynamics are learned, we use it to develop an MPC-style safe navigation controller.

low-dimensional, component-wise dynamics, which may not sufficiently capture the nonlinearity of high-level behaviors in more challenging scenarios.

In this work, we leverage Koopman operator theory to represent the nonlinear dynamics of bipedal robots as linear transitions in a high-dimensional lifted space [14], [15]. We first train a low-level locomotion policy via deep reinforcement learning and then capture its low-frequency, base-level dynamics using Dynamic Mode Decomposition (DMD). Unlike existing approaches that rely on simplified analytic models or black-box neural networks, our framework provides a simple yet accurate representation of dynamics. Building on this model, we formulate an MPC framework using a standard quadratic objective and a linear dynamics constraint, enabling both computational efficiency and reliable performance for safety-critical navigation tasks.

We conducted experiments to evaluate the effectiveness of our framework. In terms of long-term prediction accuracy, both Koopman-based models consistently outperformed a component-wise linear model [13], a simple linear integrator, and a unified linear model, with the Koopman-based model achieving the highest accuracy. We further assessed each model’s ability to support safe navigation of a G1 humanoid when combined with MPC across four maps of varying difficulty (Fig. 2). Our results demonstrate that the Koopman model enabled reliable safe navigation by achieving higher success rates compared to the baselines. The main contributions of this work are:

- We propose a novel Koopman-based safe navigation

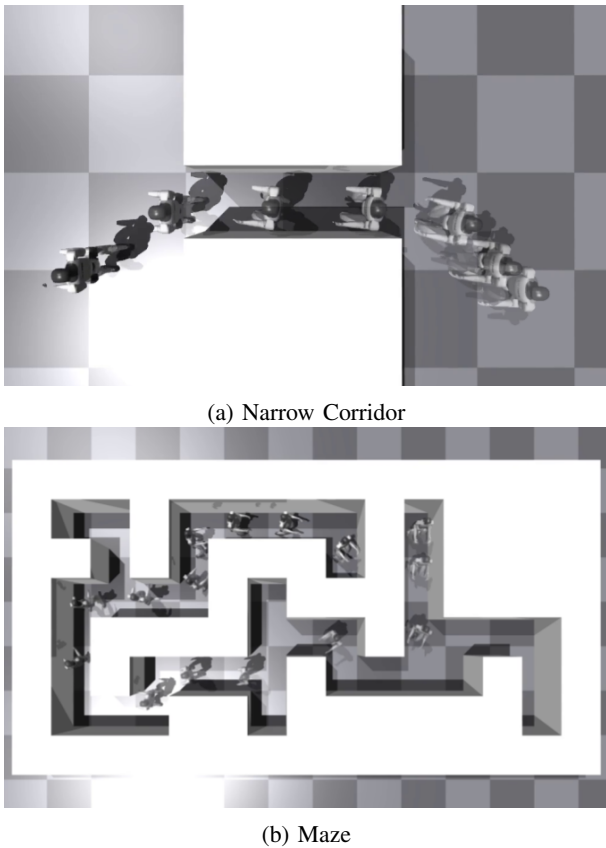


Fig. 2: Our approach enables safe navigation in challenging environments with dense obstacles and narrow passages.

control framework for bipedal robots, which leverages learned linear Koopman dynamics and model-predictive control.

- We provide a comprehensive evaluation of various forward dynamics models on bipedal robots, including an integrator, component-wise linear model, a unified linear model, and Koopman dynamics models with different lifting functions.
- We demonstrate improved safety of the proposed framework compared to the baselines.

II. RELATED WORKS

A. Safe Legged Locomotion

It is important to ensure safety during legged robots' dynamic motions with underactuated bases. Previously, safety has been widely discussed within the context of model-based control [2], [16]. Recent advances in learning-based locomotion frameworks [17], [18] have demonstrated impressive robustness, but there are only limited works that discuss the interpretability [19] and guarantee of safety [20]. A common approach in this context is to decouple a low-level locomotion controller and a high-level navigation policy, where a high-level policy adopts conventional methods such as model predictive control and control barrier functions [21]–[23]. Li et al. [13] propose a method that leverages low-dimensional linear models identified from bipedal locomotion policies trained via reinforcement learning. Liao et al. [24] models

robots and obstacles as polytopes [25] to enable narrow space navigation. However, they require access to a low-level whole-body controller, which is not available in many real-world scenarios. Instead of using analytic formulations, there exist works to model low-level behaviors using neural networks [26], [27]. However, the learned dynamics are often highly nonlinear, which makes it infeasible to adopt conventional optimization methods and requires additional techniques, such as an informed trajectory sampler [27].

B. Koopman Operator for Robotics

The Koopman operator theory [28], which offers a linear perspective on nonlinear dynamical systems, has gained growing interest in robotics for its potential to simplify complex dynamical systems [29] and high sample efficiency [30]. They have been successfully utilized in various domains such as spherical robots [29], drones [31]–[33], and dexterous manipulation [30], [34], [35]. Leveraging their linearity, Koopman operator methods have widely been combined with model predictive control to obtain desired command tracking [29], [36], enforce better stability, or improve safety. The Koopman operator has also proven useful in learning the reference dynamics from trajectory data, which demonstrates superior sample efficiency compared to deep neural networks in dexterous manipulation [30]. In this work, we learn the high-level dynamics of the velocity-tracking policy and leverage a model predictive control framework to obtain safe commands to navigate within environments with obstacles.

III. PRELIMINARIES: LEARNING KOOPMAN DYNAMICS

This section introduces Koopman operator theory, a framework that enables representing nonlinear dynamics through linear evolution in a lifted space [15].

1) *Koopman Representation*: Consider a nonlinear system $x_{t+1} = F(x_t)$, where $x_t \in \mathcal{X} \subset \mathbb{R}^n$ denotes the state at time t , and $F(\cdot) : \mathbb{R}^n \rightarrow \mathbb{R}^n$ is a nonlinear transition function. We introduce a set of *observables* using the so-called *lifting function* $\psi : \mathcal{X} \rightarrow \mathcal{O}$, where \mathcal{O} denotes the space of observables, to capture nonlinear dynamics as linear relationships between observables. We define the Koopman operator \mathcal{K} acting on an observable function ψ as:

$$(\mathcal{K}\psi)(x_t) = \psi(F(x_t)) = \psi(x_{t+1}).$$

If the observables form a vector space, \mathcal{K} can be regarded as an *infinite-dimensional linear operator* that governs their evolution: $\psi(x_{t+1}) = \mathcal{K}\psi(x_t)$.

In practice, this representation is not directly useful because it is infinite-dimensional, which makes computation infeasible. To address this limitation, we approximate \mathcal{K} with a finite-dimensional matrix $K \in \mathbb{R}^{p \times p}$ and define a corresponding finite set of observables $\psi(t) \in \mathbb{R}^p$. The system can then be represented as $\psi(x_{t+1}) = K\psi(x_t) + r(x_t)$, where $r(x_t) \in \mathbb{R}^p$ is the residual error caused by the finite-dimensional approximation. This error can be reduced by appropriately selecting the lifting function, the dimension p , and the mapping $\psi(\cdot)$.

In addition, we can illustrate a controlled dynamical system $x_{t+1} = F(x_t, u_t)$, with a control $u_t \in \mathcal{U} \subset \mathbb{R}^m$, which yields $\psi(x_{t+1}, u_{t+1}) = \mathcal{X} \psi(x_t, u_t)$. A common strategy [29] is to design $\psi(\cdot)$ by lifting states with a state-specific function $\phi(\cdot)$ and concatenating them with the control signal $\psi(x_t, u_t) = [\phi(x_t); u_t]$, which yields:

$$[\phi(x_{t+1}); u_{t+1}] = K[\phi(x_t); u_t] + r(x_t, u_t).$$

If we skip control prediction, we obtain:

$$\phi(x_{t+1}) = A\phi(x_t) + Bu_t + r(x_t, u_t).$$

2) *Learning Koopman Dynamics*: The matrix operators K can be learned from a dataset $\mathcal{D} = [(x_1, u_1), \dots, (x_T, u_T)]$, which contains the state trajectories and control inputs. Given the choice of state observables $\phi(\cdot)$, K can be computed by minimizing the cost function J :

$$J(K) = \sum_{t=1}^{t=T-1} \|r(x_t, u_t)\|^2 = \sum_{t=1}^{t=T-1} \|[\phi(x_{t+1}); u_{t+1}] - K[\phi(x_t); u_t]\|^2. \quad (1)$$

Because this is a least-square problem, we can simply obtain an analytical solution. We can define X and Y as:

$$X = \frac{1}{T-1} \sum_{t=1}^{t=T-1} [\phi(x_{t+1}); u_{t+1}] \otimes [\phi(x_t); u_t]$$

$$Y = \frac{1}{T-1} \sum_{t=1}^{t=T-1} [\phi(x_t); u_t] \otimes [\phi(x_t); u_t],$$

where \otimes denotes the outer product. Then, we can take the Moore-Penrose inverse $K = XY^\dagger$ as suggested in [14], [37].

IV. SAFE NAVIGATION WITH LEARNED KOOPMAN FORWARD DYNAMICS

This section presents a novel safe navigation framework that leverages the learned Koopman dynamics. Model-predictive control (MPC) has been widely adopted as a theoretical backbone for safe navigation. However, the high-level forward dynamics of a bipedal robot are difficult to analyze because it is a closed-loop system with a nonlinear control policy and hybrid contact dynamics, which can degrade the performance of the existing safety-aware control algorithms.

Instead, we capture a robot's high-level forward dynamics as a linear evolution of high-dimensional features by adopting the Koopman operator theory. Due to its linearity, this enables effective integration with the existing MPC-based safe navigation algorithms.

A. Low-level Locomotion Controller

Our framework assumes a velocity-tracking controller that takes as input the target velocity and outputs motor commands. While high-level dynamics learning can be agnostic to the implementation of a low-level controller, we opt for deep RL that can learn a robust control policy from a relatively simple reward function.

Following the reward structure from [38], we train a locomotion controller for the Unitree G1 robot [39] using Proximal Policy Optimization (PPO) [40]. The low-level control policy $\pi_\theta(a_t | o_t)$ maps proprioceptive observations

o_t to actions $a_t \in \mathbb{R}^{12}$, which correspond to target joint angles for the 12 lower body joint actuators. A PD controller then converts these targets into torques using joint-specific stiffness and damping gains. The policy observes $o_t \in \mathbb{R}^{47}$:

$$o_t = [\omega_t, g_t, \hat{v}, q, \dot{q}_t, a_{t-1}, \sin(2\pi c_t), \cos(2\pi c_t)]$$

The observation vector consists of the base angular velocity $\omega_t \in \mathbb{R}^3$, the projected gravity vector $g_t \in \mathbb{R}^3$, and the command linear and angular velocities $\hat{v} = [\hat{v}_x, \hat{v}_y, \hat{\omega}] \in \mathbb{R}^3$. It further includes the joint positions and velocities $q, \dot{q} \in \mathbb{R}^{12}$, together with the previous action $a_{t-1} \in \mathbb{R}^{12}$. To aid in learning rhythmic gaits, a 2D gait phase clock $[\sin(2\pi c_t), \cos(2\pi c_t)]$ is included, where the phase clock c_t cycles with a period of 0.8 seconds. The policy is modeled using a recurrent neural network(LSTM).

Training is performed in the IsaacGym simulator [41] with 4,096 parallel environments for 7,000 steps, requiring approximately two hours on an NVIDIA RTX 4090 GPU.

B. Data Collection for High-level Dynamics

We create the dataset of high-level floating base movements by generating 150 locomotion trajectories. Each trajectory consists of 150 seconds of robot state recorded at 50 Hz, which results in 7500 data points for each trajectory. We obtain diverse and dynamic trajectories by randomly sampling velocity commands every 0.5 seconds. For each trajectory, we record the high level states of the robot state: $x = [p_x, p_y, \theta, v_x, v_y, \omega]$, where p_x, p_y, θ are x, y coordinates and direction heading of the robot and v_x, v_y, ω are x, y linear velocity components and z -axis angular velocity of the robot. We also record the velocity tracking commands given to the robot: $u = [\hat{v}_x, \hat{v}_y, \hat{\omega}]$, where the commands are relative to the position and orientation of robot's state at each step.

For better coverage, we apply a data augmentation technique by applying transformations to the existing dataset. For each episode of length N state transitions $[x_0, u_0, \dots, u_{N-1}, x_N]$, we extract sequences of length H , leading to $(N - H + 1)$ sequences per N step trajectory. For each sequence of length H , we convert the positional and angular components to the coordinate of its first state.

Formally, for i -th state sequence of an episode: $[x_i, \dots, x_{i+H}]$, we convert each state represented in a global coordinate to the local coordinate system with respect to the first state x_i . This will lead to a representation of $[x_i^l, \dots, x_{i+H}^l]$, where x_j^l represents a x_j represented in the frame of x_i . As a result, we obtain the final dataset \mathcal{D} which contains 236,250 frames of state transitions.

C. Learning high-level dynamics

Our main objective in this section is to learn the state transition function $x_{t+1} = F(x_t, u_t)$, where $F(\cdot) : \mathcal{X} \times \mathcal{U} \rightarrow \mathcal{X}$ is a high-level dynamics that governs the closed-loop dynamics of nonlinear legged locomotion.

One key challenge in learning F is that it can be arbitrarily nonlinear. One potential way in machine learning to learn the transition function F is to utilize a universal function approximator, a multi-layer perceptron (MLP), to model

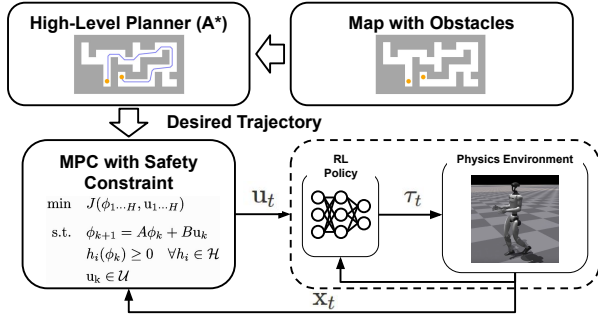


Fig. 3: Overview of the navigation framework.

the input-output mapping of the function F minimizing the L_2 loss: $\|x_{t+1} - f_{MLP}(x_t, u_t)\|_2$ for $\forall t$. However, utilizing MLP dynamics constraint in the MPC framework causes practical challenges, which makes MLP-learned dynamics impractical for general usage. For instance, Direct Multiple Shooting formulation [25], [42], [43], one of the widely used techniques in solving MPC, requires the dynamics constraint containing MLP to match for every time step, making the optimization extremely nonconvex. As a result, nonlinear solvers often fail to solve the optimization with MLP dynamics constraints.

Instead, we use the Koopman operator’s linear evolution to represent dynamics in the lifted space, which makes the dynamics constraint in the MPC framework linear. As a result, our approach offers the possibility of adopting linear MPC with control barrier functions. In this work, we use the Koopman forward dynamics as described in Section. III: $\phi(x_{t+1}) = A\phi(x_t) + Bu_t$, where the state-lifting, $\phi(\cdot) : \mathbb{R}^n \rightarrow \mathbb{R}^{n'}$ $n' \geq n$, is a vector-valued lifting function. Inspired by [30], the first n elements of the $\phi(x_t)$ are x_t so that we can easily retrieve the original states, which are used for computing obstacle-avoidance constraints. Note that in the case of $n' = n$, $\phi(x)$ becomes the same as x , and the solutions A and B becomes a linear identification of the high-level dynamics. Finally, we obtain the *analytical* solution A and B matrices by solving the optimal solution of $J(K)$ in Equation. 1, which in general only takes seconds of CPU-only computation.

D. Safe Navigation with Koopman-based MPC

Once we obtain the learned linear evolution in the lifting space, we can incorporate the existing control framework for high-level tasks. In our case, we leverage the existing linear Model-Predictive Control algorithm to design the safety-guaranteed legged navigation controller. The overview is illustrated in Fig. 3. Our optimization can be formulated as follows:

$$\begin{aligned}
 \min_{\phi_{1..H}, u_{1..H}} \quad & J(\phi_{1..H}, u_{1..H}) \\
 \text{s.t.} \quad & \phi_{k+1} = A\phi_k + Bu_k \quad \forall k = 0, \dots, H-1 \\
 & h_i(\phi_k) \geq 0 \quad \forall h_i \in \mathcal{H} \text{ and } \forall k = 1, \dots, H \\
 & u_k \in \mathcal{U}.
 \end{aligned}$$

The key idea of our framework is to directly solve lifted variables $\phi_{1..H}$, instead of the original states $x_{1..H}$, along with control variables $u_{1..H}$. This formulation is effective because all the dynamics become linear in the lifted space.

Our objective function is designed to track the given trajectory $\hat{x}_{1..H}$ in the original state space:

$$J(\phi_{1..H}, u_{1..H}) = \sum_{k=1}^H \|x_k - \hat{x}_k\|_p + \sum_{k=0}^{H-1} \|u_{k+1} - u_k\|_2,$$

where the $x_k = \phi^{-1}(\phi_k)$ for all the timestep k . Designing the lifting function ϕ to include the original state information, the inverse operation $\phi^{-1}(\cdot)$ becomes a linear projection, making the cost function to be quadratic with respect to all the variables.

The first constraint aims to satisfy the learned dynamics. The second constraint is an arbitrary task-specific constraint, in our case, a distance barrier function $h_i(\phi_k) = \hat{\text{dist}}(x_k, \text{obstacle}_i)$ for all obstacles. The third constraint confines control signals within the valid region.

Note that this formulation can readily incorporate safety frameworks such as discrete control barrier functions [44], by modifying direct collision checking $\hat{h}(x_k) \geq 0$ constraint to that of control barrier function: $\hat{h}(x_{k+1}) \geq \gamma \hat{h}(x_k)$ for $\gamma \in [0, 1)$, which can still be linear based on obstacle geometry and choice of barrier function \hat{h} .

V. EXPERIMENTAL EVALUATION

We evaluated our method along with baselines in terms of the long-term forward prediction accuracy (Sec. V-B) and the MPC-based safe navigation performance (Sec. V-C).

A. Experimental Design

We collected all locomotion data and tested the navigation performance using the Unitree G1 [39] robot built with IsaacGym simulator [41]. The MPC optimization is solved using IPOPT interfaced through CasADi [45].

We compared various *Koopman Dynamics* models along with the baselines:

Integrator: An ideal first-order model: $[p_x, p_y, \theta]_{t+1} = [p_x, p_y, \theta]_t + dt[v_x, v_y, \omega]_t$; $[v_x, v_y, \omega]_{t+1} = [\hat{v}_x, \hat{v}_y, \hat{\omega}]_t$, where $dt = 0.02s$ represents the duration of one simulation step and with the velocities accumulated in the global frame. Note that this baseline does not require data for training.

Component-wise Linear (Comp.Lin.): Building on the baseline in [13], we learn a block-structured linear model by assuming independence among the components in the state dynamics.

Unified Linear (Linear): This baseline assumes $\phi(x) = x$ (i.e., no other lifting functions), indicating a linear system evolution under control inputs in the original state space. Similarly, these matrices are learned from the dataset \mathcal{D} .

Multi-layer Perceptron (MLP): We train MLP to learn the input and output of the transition function, as described in Sec. IV-C. Our network has two hidden layers of [32, 32] with a ReLU activation function.

Koopman: Our Koopman dynamics model has been tested with various lifting functions, including polynomial, cross,

Model	MSE	RMSE	Training Time (s)	Lifted Dim	RMSE X (m)	RMSE Y (m)	RMSE Yaw (rad)
Koopman Lifting Models							
Koopman (Poly2+Cross+Trig+Bilin)	0.027	0.166	0.45	61	0.089	0.097	0.116
Koopman (Poly2+Cross+Bilin)	0.028	0.166	0.31	49	0.089	0.098	0.117
Koopman (MLP, 16)	0.028	0.167	205.3	16	0.078	0.087	0.141
Koopman (MLP, 24)	0.028	0.167	206.3	24	0.077	0.088	0.141
Koopman (Poly3+Cross+Trig)	0.029	0.170	0.326	49	0.094	0.101	0.138
Koopman (Poly2+Cross+Trig)	0.029	0.170	0.259	43	0.094	0.101	0.141
Koopman (Poly3+Cross)	0.029	0.170	0.231	37	0.094	0.101	0.141
Koopman (Poly2+Cross)	0.029	0.170	0.156	31	0.094	0.102	0.142
Baseline Models							
Linear	0.033	0.182	0.010	—	0.140	0.149	0.144
Component-wise Linear	0.034	0.183	0.020	—	0.140	0.149	0.144
MLP	0.036	0.189	142.2	—	0.147	0.153	0.148
Integrator	0.083	0.289	—	—	0.178	0.173	0.236

TABLE I: Average *prediction error* on the validation dataset. The best performance is highlighted in bold.

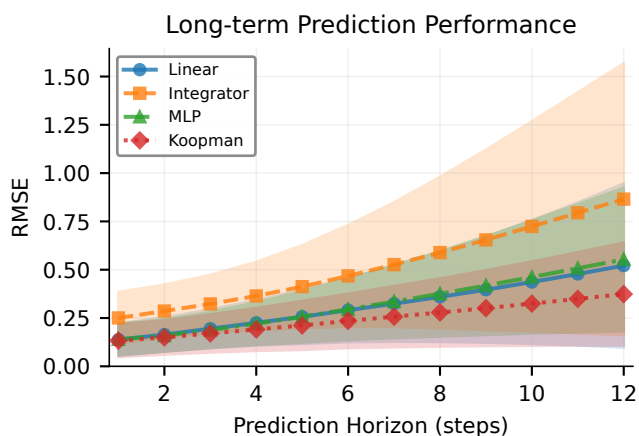


Fig. 4: Long-term prediction error across the entire validation set. The bold line indicates the mean, and the shaded region shows the standard deviation.

bilinear, and trigonometric terms. We also investigated MLP-based feature lifting functions, which simultaneously learns MLP feature layers and the transition matrix similar to the training process of the MLP model.

B. Long-term Forward Prediction

We train various Koopman dynamics models and compare them against several baselines, as summarized in Table I. The evaluation metrics include MSE, RMSE, training time, lifted dimension, and selected per-dimension RMSE for interpretability. Note that RMSE is computed in the 6D space for all the position and velocity values. Overall, these results demonstrate that Koopman lifting consistently outperforms baseline approaches in predictive accuracy. The full Koopman model with polynomial, cross, bilinear, and trigonometric observables attains the best RMSE score of 0.166. Even the weakest Koopman variant with polynomial and cross terms achieves an RMSE of 0.170, outperforming the most accurate baseline model, *Linear*, with an RMSE of 0.182. While the Koopman model with learned MLP features yields the lowest RMSE along the X and Y directions, its inherent nonlinearity may complicate the MPC optimization process in the following section.

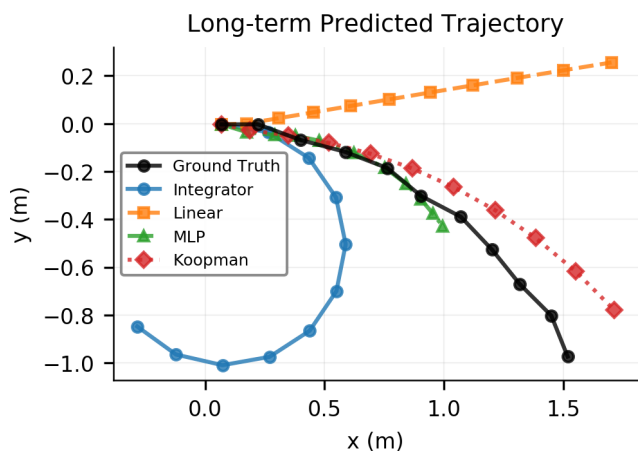


Fig. 5: Comparison of a long-term prediction of Koopman model against the baselines ($\Delta t = 0.5$). The ground-truth trajectory is generated from a constant command not included in the training dataset. Koopman Forward Dynamics achieve two to four times less final step error compared to *Linear* and *MLP* baselines.

For the remainder of the experiments, we adopt the *Koopman (Poly3+Cross+Trig)* model, which achieves competitive performance while strictly adhering to the setup in Section III of $\psi(x_t, u_t) = [\phi(x_t), u_t]$; in particular, no bilinear state-control terms $x_i u_j$ are included in the lifting.

Although the performance gain reported in Table I may appear small, we want to note that they correspond to single-step predictions, and such errors accumulate rapidly in long-horizon rollouts. Fig. 4 presents long-term prediction errors across the validation set, where trajectories are predicted for 12 steps (6 seconds) using different models. While all models start with similar errors around 0.15, the Koopman model achieves a significantly lower long-term error of 0.37 after 12 steps, compared to 0.55 and 0.52 for the MLP and linear models, respectively. These results highlight the superior long-term prediction accuracy of the learned Koopman dynamics.

Fig. 5 illustrates a representative trajectory from the validation set, comparing predictions from *Koopman*, *MLP*,

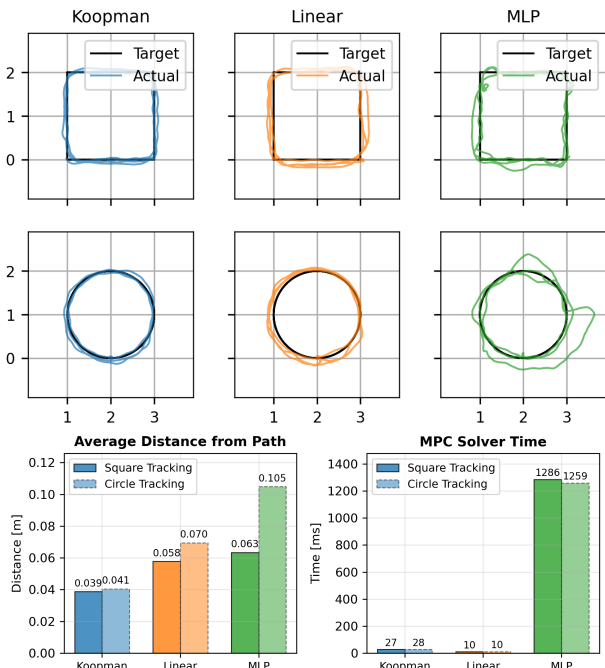


Fig. 6: Comparison of path-tracking trajectories (top), average distance from the reference path (bottom left), and solver time (bottom right).

linear, and *integrator* models. While the baseline models deviate significantly after only a few steps, the Koopman model closely follows the ground-truth trajectory and achieves a final-step error that is two to four times lower than the others.

C. MPC-based Safe Navigation

In this section, we evaluate the performance of the proposed safe navigation framework (Sec. IV-D). We first evaluate path-tracking accuracy in obstacle-free environments and then examine navigation performance in corridor and maze environments.

1) *Pathtracking in obstacle free environments*: We compare safe navigation with the *Koopman* model against two baselines: *Linear* and *MLP*. The *Linear* model is included as the best-performing baseline, while the *MLP* model is chosen for its ability to capture nonlinear dynamics. The three models are evaluated on two trajectories, a square and a circle, both involving multiple turns. Fig. 6 shows the reference and actual trajectories (top), along with the average distance from the reference path (bottom left) and the MPC solver time (bottom right).

In our experiments, we observe that navigation with the *Koopman* model achieves the best overall performance, as its trajectories almost overlap with the reference paths. In contrast, the *Linear* model shows noticeable deviations, particularly at sharp turns along the edges, highlighting its difficulty in accurately predicting turning behavior. The *MLP*-based model performs the worst, producing unstable and erratic trajectories. This is largely because incorporating an *MLP* as the dynamics model introduces highly nonlinear constraints into the MPC optimization, making it difficult for the solver to find a stable solution in real time. Quantitatively,

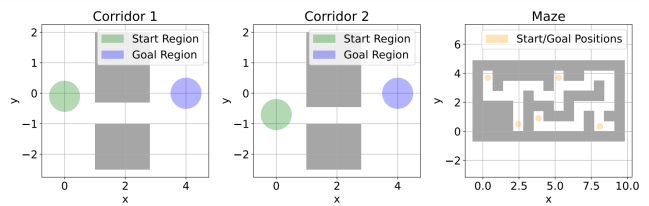


Fig. 7: Environments used for Navigation. For *corridor 1* and *corridor 2*, robots are randomly spawned in green start regions and their destination is randomly sampled from blue goal region. For *maze* environment, start and goal positions are sampled randomly in one of the 5 positions (orange).

	Corridor 1		Corridor 2		Maze 1		Maze 2	
	Time	Succ.	Time	Succ.	Time	Succ.	Time	Succ.
<i>Integrator</i>	9.48	55	9.45	60	35.5	40	35.9	40
<i>Linear</i>	7.64	75	7.83	80	33.8	40	38.0	20
<i>Koopman</i>	8.63	75	8.88	80	32.7	80	29.7	100

TABLE II: Safe navigation results in four environments, where we compare the time (s) ↓ and success rate (%) ↑.

our model achieves the lowest tracking errors of 0.039 m and 0.041 m in the square and circle tracking tasks, which correspond to 67.2% and 58.6% of the 0.058 m and 0.070 m errors of the second best model, *Linear*. These results demonstrate that the enhanced predictive accuracy of our learned *Koopman* forward dynamics directly translates into better navigation performance.

2) *Safe navigation in corridors and mazes*: In this section, we compare the navigation performance of MPC with the learned *Koopman* dynamics against the *Integrator* and *Linear* models. The *MLP* model is omitted due to its poor tracking performance and high computational cost.

We evaluate the effectiveness of the learned models in four navigation environments: *i*) *Corridor 1*, a wide corridor with a 70 cm gap; *ii*) *Corridor 2*, a narrow corridor with a 55 cm gap; *iii*) *Maze 1*, an artifact maze [25] with 0.9 m passages; and *iv*) *Maze 2*, the same maze with narrower passages of 0.8 m. For each environment, we randomize start and goal positions and sample five pairs. To isolate planning performance from perception, we assume obstacle positions and shapes are known. A high-level planner generates rough waypoints using the A* algorithm [46], which serve as reference trajectories for the MPC controller.

We measure the seconds taken to reach destination and the success rate of the navigation and report them in Table II. Here, the success is determined based on whether the robot was able to reach the destination in a desired time window, where we give 10 seconds for corridors and 40 seconds for maze environments. We did not terminate the episode upon minor collisions. However, when the robot fell down and was not able to recover, we marked them as failure cases.

Overall, navigation with the *Koopman* model achieves the best performance, attaining the highest success rates across all four environments. In particular, it reaches success rates of 80% and 100% in *Maze 1* and *Maze 2*, respectively, significantly outperforming the 40% and 20% achieved by the *Linear* model. This improvement arises because *Koop-*

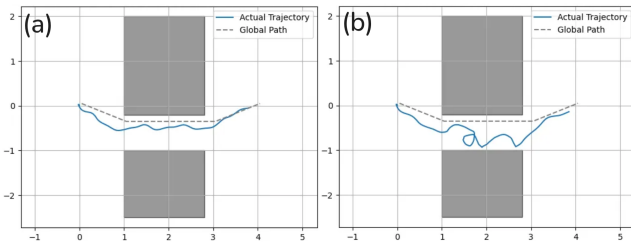


Fig. 8: Trajectory of safe navigation in *Corridor 1*. (a) The *Koopman* model successfully passes through the corridor without collision, while (b) the *Linear* baseline collides with the walls.

man models are better at capturing turning motions compared to the baselines, and the *maze* environment requires frequent turning to complete the task. However, in terms of completion time in both *Corridor 1* and *Corridor 2*, the *Koopman* models achieve the second-best performance, while the *Linear* model shows the fastest travel time. We observed that in some runs, collisions in the *Linear* model triggered aggressive behavior, allowing the robot to reach the target more quickly. However, this behavior is detrimental in the maze task, where successful navigation requires precise handling of complex turns.

Fig. 8 illustrates a representative scenario in *Corridor 1* by comparing the base trajectories of the *Koopman* and *Linear* models. The accurate predictive capability of the learned *Koopman* dynamics enables MPC-based navigation to follow the reference trajectory closely while avoiding collisions with nearby obstacles. In contrast, navigation with the *Linear* model overshoots at turns and results in severe collisions with the wall. These results highlight the potential of *Koopman*-based dynamics to improve safety in complex navigation tasks.

VI. CONCLUSION AND FUTURE WORK

In this work, we present a novel safe navigation framework for bipedal robots by combining *Koopman* operator theory with the MPC framework. We first train a low-level locomotion control policy using deep RL. Then, we learn the nonlinear base-level dynamics from the collected trajectories using Dynamic Mode Decomposition. Finally, we develop an MPC framework for safe navigation that efficiently solves the given constrained optimization problem by leveraging the linearity of the learned *Koopman* dynamics. We show that the learned *Koopman* dynamics offer improved accuracy for long-term forward dynamics prediction. We also deploy our safe navigation framework in challenging environments with narrow passages and mazes and demonstrate improved safety compared to the baselines.

There are several directions for future work. For instance, the utility of the learned linear dynamics is not limited to obstacle avoidance discussed in this work. There exists a wide range of potential tasks, such as loco-manipulation, or traversing more complex environments, which require modeling full-body dynamics. This goal will likely require a careful investigation of the lifting function for the reliable

Koopman linearization. We also aim to extend the capability of this method by exploring diverse lifting techniques. One possibility is to utilize time-delay or recurrent neural network based lifting, which could provide a more concise and accurate forward dynamics model. However, this may introduce additional complexity into the implementation of the learning framework. Investigating this trade-off will be an interesting future research direction for legged robots. Finally, the learned linearized model may show severe performance degradation in unseen environments and lead to the failure of safe navigation. It will be interesting to combine our framework with additional safety mechanisms, such as control barrier functions under state uncertainty [47] or additional recovery controllers [48].

REFERENCES

- [1] S. Tonneau, A. Del Prete, J. Pettré, C. Park, D. Manocha, and N. Mansard, “An efficient acyclic contact planner for multiped robots,” *IEEE Transactions on Robotics*, vol. 34, no. 3, pp. 586–601, 2018.
- [2] J. Di Carlo, P. M. Wensing, B. Katz, G. Bleedt, and S. Kim, “Dynamic locomotion in the mit cheetah 3 through convex model-predictive control,” in *2018 IEEE/RSJ International Conference on Intelligent Robots and Systems (IROS)*. IEEE, 2018, pp. 1–9.
- [3] L. Wellhausen and M. Hutter, “Rough terrain navigation for legged robots using reachability planning and template learning,” in *2021 IEEE/RSJ International Conference on Intelligent Robots and Systems (IROS)*. IEEE, 2021, pp. 6914–6921.
- [4] M. Asselmeier, J. Ivanova, Z. Zhou, P. A. Vela, and Y. Zhao, “Hierarchical experience-informed navigation for multi-modal quadrupedal rebar grid traversal,” in *2024 IEEE International Conference on Robotics and Automation (ICRA)*. IEEE, 2024, pp. 8065–8072.
- [5] J. Merel, A. Ahuja, V. Pham, S. Tunyasuvunakool, S. Liu, D. Tirumala, N. Heess, and G. Wayne, “Hierarchical visuomotor control of humanoids,” *arXiv preprint arXiv:1811.09656*, 2018.
- [6] D. Hoeller, L. Wellhausen, F. Farshidian, and M. Hutter, “Learning a state representation and navigation in cluttered and dynamic environments,” *IEEE Robotics and Automation Letters*, vol. 6, no. 3, pp. 5081–5088, 2021.
- [7] D. Hoeller, N. Rudin, D. Sako, and M. Hutter, “Anymal parkour: Learning agile navigation for quadrupedal robots,” *Science Robotics*, vol. 9, no. 88, p. eadi7566, 2024.
- [8] R. Yang, G. Yang, and X. Wang, “Neural volumetric memory for visual locomotion control,” in *Proceedings of the IEEE/CVF Conference on Computer Vision and Pattern Recognition*, 2023, pp. 1430–1440.
- [9] Z. Zhuang, Z. Fu, J. Wang, C. Atkeson, S. Schwertfeger, C. Finn, and H. Zhao, “Robot parkour learning,” *arXiv preprint arXiv:2309.05665*, 2023.
- [10] X. Cheng, K. Shi, A. Agarwal, and D. Pathak, “Extreme parkour with legged robots,” in *2024 IEEE International Conference on Robotics and Automation (ICRA)*. IEEE, 2024, pp. 11 443–11 450.
- [11] Z. Xie, X. Da, B. Babich, A. Garg, and M. v. de Panne, “Glide: Generalizable quadrupedal locomotion in diverse environments with a centroidal model,” in *International workshop on the algorithmic foundations of robotics*. Springer, 2022, pp. 523–539.
- [12] H. Jung, Z. Gu, Y. Zhao, H.-W. Park, and S. Ha, “Ppf: Pre-training and preservative fine-tuning of humanoid locomotion via model-assumption-based regularization,” *IEEE Robotics and Automation Letters*, 2025.
- [13] Z. Li, J. Zeng, A. Thirugnanam, and K. Sreenath, “Bridging model-based safety and model-free reinforcement learning through system identification of low dimensional linear models,” *arXiv preprint arXiv:2205.05787*, 2022.
- [14] P. J. Schmid, “Dynamic mode decomposition of numerical and experimental data,” *Journal of fluid mechanics*, vol. 656, pp. 5–28, 2010.
- [15] B. O. Koopman, “Hamiltonian Systems and Transformation in Hilbert Space,” *Proceedings of the National Academy of Sciences*, vol. 17, no. 5, pp. 315–318, 1931.
- [16] A. W. Winkler, C. D. Bellicoso, M. Hutter, and J. Buchli, “Gait and trajectory optimization for legged systems through phase-based end-effector parameterization,” *IEEE Robotics and Automation Letters*, vol. 3, no. 3, pp. 1560–1567, 2018.

- [17] T. Haarnoja, A. Zhou, K. Hartikainen, G. Tucker, S. Ha, J. Tan, V. Kumar, H. Zhu, A. Gupta, P. Abbeel *et al.*, “Soft actor-critic algorithms and applications,” *arXiv preprint arXiv:1812.05905*, 2018.
- [18] N. Rudin, D. Hoeller, P. Reist, and M. Hutter, “Learning to walk in minutes using massively parallel deep reinforcement learning,” in *Conference on Robot Learning*. PMLR, 2022, pp. 91–100.
- [19] C. Glanois, P. Weng, M. Zimmer, D. Li, T. Yang, J. Hao, and W. Liu, “A survey on interpretable reinforcement learning,” *Machine Learning*, pp. 1–44, 2024.
- [20] T. He, C. Zhang, W. Xiao, G. He, C. Liu, and G. Shi, “Agile but safe: Learning collision-free high-speed legged locomotion,” *arXiv preprint arXiv:2401.17583*, 2024.
- [21] A. D. Ames, S. Coogan, M. Egerstedt, G. Notomista, K. Sreenath, and P. Tabuada, “Control barrier functions: Theory and applications,” in *2019 18th European control conference (ECC)*. IEEE, 2019, pp. 3420–3431.
- [22] R. Grandia, A. J. Taylor, A. D. Ames, and M. Hutter, “Multi-layered safety for legged robots via control barrier functions and model predictive control,” in *2021 IEEE International Conference on Robotics and Automation (ICRA)*. IEEE, 2021, pp. 8352–8358.
- [23] J. Choi, F. Castaneda, C. J. Tomlin, and K. Sreenath, “Reinforcement learning for safety-critical control under model uncertainty, using control lyapunov functions and control barrier functions,” *arXiv preprint arXiv:2004.07584*, 2020.
- [24] Q. Liao, Z. Li, A. Thirugnanam, J. Zeng, and K. Sreenath, “Walking in narrow spaces: Safety-critical locomotion control for quadrupedal robots with duality-based optimization,” in *2023 IEEE/RSJ International Conference on Intelligent Robots and Systems (IROS)*. IEEE, 2023, pp. 2723–2730.
- [25] A. Thirugnanam, J. Zeng, and K. Sreenath, “Safety-critical control and planning for obstacle avoidance between polytopes with control barrier functions,” in *2022 International Conference on Robotics and Automation (ICRA)*. IEEE, 2022, pp. 286–292.
- [26] J. Kim, T. Li, and S. Ha, “Armp: Autoregressive motion planning for quadruped locomotion and navigation in complex indoor environments,” in *2023 IEEE/RSJ International Conference on Intelligent Robots and Systems (IROS)*. IEEE, 2023, pp. 2731–2737.
- [27] Y. Kim, C. Kim, and J. Hwangbo, “Learning forward dynamics model and informed trajectory sampler for safe quadruped navigation,” *arXiv preprint arXiv:2204.08647*, 2022.
- [28] B. O. Koopman and J. v. Neumann, “Dynamical systems of continuous spectra,” *Proceedings of the National Academy of Sciences*, vol. 18, no. 3, pp. 255–263, 1932.
- [29] I. Abraham, G. De La Torre, and T. D. Murphey, “Model-based control using koopman operators,” *arXiv preprint arXiv:1709.01568*, 2017.
- [30] Y. Han, M. Xie, Y. Zhao, and H. Ravichandar, “On the utility of koopman operator theory in learning dexterous manipulation skills,” in *Conference on Robot Learning*. PMLR, 2023, pp. 106–126.
- [31] C. Folkestad, S. X. Wei, and J. W. Burdick, “Koopnet: Joint learning of koopman bilinear models and function dictionaries with application to quadrotor trajectory tracking,” in *2022 International Conference on Robotics and Automation (ICRA)*. IEEE, 2022, pp. 1344–1350.
- [32] C. Folkestad and J. W. Burdick, “Koopman nmpc: Koopman-based learning and nonlinear model predictive control of control-affine systems,” in *2021 IEEE International Conference on Robotics and Automation (ICRA)*. IEEE, 2021, pp. 7350–7356.
- [33] C. Folkestad, Y. Chen, A. D. Ames, and J. W. Burdick, “Data-driven safety-critical control: Synthesizing control barrier functions with koopman operators,” *IEEE Control Systems Letters*, vol. 5, no. 6, pp. 2012–2017, 2020.
- [34] Y. Han, Z. Chen, K. A. Williams, and H. Ravichandar, “Learning prehensile dexterity by imitating and emulating state-only observations,” *IEEE Robotics and Automation Letters*, 2024.
- [35] H. Chen, A. Abuduweili, A. Agrawal, Y. Han, H. Ravichandar, C. Liu, and J. Ichnowski, “Korol: Learning visualizable object feature with koopman operator rollout for manipulation,” *arXiv preprint arXiv:2407.00548*, 2024.
- [36] M. Korda and I. Mezić, “Linear predictors for nonlinear dynamical systems: Koopman operator meets model predictive control,” *Automatica*, vol. 93, pp. 149–160, 2018.
- [37] M. O. Williams, I. G. Kevrekidis, and C. W. Rowley, “A data-driven approximation of the koopman operator: Extending dynamic mode decomposition,” *Journal of Nonlinear Science*, vol. 25, no. 6, pp. 1307–1346, 2015.
- [38] U. Robotics, “unitree_rl_gym: Reinforcement Learning implementation for Unitree robots (Go2, H1, H1.2, G1),” https://github.com/unitreerobotics/unitree_rl_gym, 2024, accessed: 2025-09-15.
- [39] —, “Unitree G1 Humanoid Robot,” <https://www.unitree.com/g1/>, 2024, accessed: 2025-09-15.
- [40] J. Schulman, F. Wolski, P. Dhariwal, A. Radford, and O. Klimov, “Proximal policy optimization algorithms,” *arXiv preprint arXiv:1707.06347*, 2017.
- [41] V. Makoviychuk, L. Wawrzyniak, Y. Guo, M. Lu, K. Storey, M. Macklin, D. Hoeller, N. Rudin, A. Allshire, A. Handa *et al.*, “Isaac gym: High performance gpu-based physics simulation for robot learning,” *arXiv preprint arXiv:2108.10470*, 2021.
- [42] H. G. Bock and K.-J. Plitt, “A multiple shooting algorithm for direct solution of optimal control problems,” *IFAC Proceedings Volumes*, vol. 17, no. 2, pp. 1603–1608, 1984.
- [43] M. Giffthaler, M. Neunert, M. Stäubli, J. Buchli, and M. Diehl, “A family of iterative gauss-newton shooting methods for nonlinear optimal control,” in *2018 IEEE/RSJ International Conference on Intelligent Robots and Systems (IROS)*. IEEE, 2018, pp. 1–9.
- [44] J. Zeng, B. Zhang, and K. Sreenath, “Safety-critical model predictive control with discrete-time control barrier function,” in *2021 American Control Conference (ACC)*. IEEE, 2021, pp. 3882–3889.
- [45] J. A. E. Andersson, J. Gillis, G. Horn, J. B. Rawlings, and M. Diehl, “CasADi – A software framework for nonlinear optimization and optimal control,” *Mathematical Programming Computation*, vol. 11, no. 1, pp. 1–36, 2019.
- [46] P. E. Hart, N. J. Nilsson, and B. Raphael, “A formal basis for the heuristic determination of minimum cost paths,” *IEEE transactions on Systems Science and Cybernetics*, vol. 4, no. 2, pp. 100–107, 1968.
- [47] R. K. Cosner, A. W. Singletary, A. J. Taylor, T. G. Molnar, K. L. Bouman, and A. D. Ames, “Measurement-robust control barrier functions: Certainty in safety with uncertainty in state,” in *2021 IEEE/RSJ International Conference on Intelligent Robots and Systems (IROS)*. IEEE, 2021, pp. 6286–6291.
- [48] T.-Y. Yang, T. Zhang, L. Luu, S. Ha, J. Tan, and W. Yu, “Safe reinforcement learning for legged locomotion,” in *2022 IEEE/RSJ International Conference on Intelligent Robots and Systems (IROS)*. IEEE, 2022, pp. 2454–2461.